

Ultrafast plasmonics using transparent conductive oxide hybrids in the epsilon near-zero regime.

Daniel Traviss,¹ Roman Bruck,¹ Ben Mills,² Martina Abb,¹ and Otto L. Muskens¹

¹*Physics and Astronomy, Faculty of Physical and Applied Sciences,
University of Southampton, Highfield, Southampton SO17, 1BJ, United Kingdom*

²*Optoelectronics Research Centre, Faculty of Physical and Applied Sciences,
University of Southampton, Highfield, Southampton SO17, 1BJ, United Kingdom*

(Dated: October 15, 2018)

The dielectric response of transparent conductive oxides near the bulk plasmon frequency is characterized by a refractive index less than vacuum. In analogy with x-ray optics, it is shown that this regime results in total external reflection and air-guiding of light. In addition, the strong reduction of the wavevector in the ITO below that of free space enables a new surface plasmon polariton mode which can be excited without requiring a prism or grating coupler. Ultrafast control of the surface plasmon polariton mode is achieved with a modulation amplitude reaching 20%.

Epsilon-Near Zero (ENZ) materials are a class of optical materials characterized by a real part of the dielectric function close to zero. ENZ materials are of interest for a range of applications including tailoring of directional emission and radiation phase patterns,[1–3] air-guiding of electromagnetic waves,[4] and electromagnetic tunnelling devices.[5–7] While a lot of effort is aimed at achieving an ENZ response using artificial metamaterial resonators, some naturally occurring materials also show a strong reduction of the permittivity below that of vacuum. An example of naturally occurring low-index materials are noble metals where the optical permittivity ϵ is governed by the collective motions of the free electron gas known as bulk plasmons. According to the Drude model, the permittivity is given by

$$\epsilon(\omega) = \epsilon_\infty - \frac{\omega_{\text{pl}}^2}{\omega^2 + i\omega\gamma}, \quad (1)$$

where γ denotes the damping rate of the free electrons and the plasma frequency ω_{pl} is given by $\omega_{\text{pl}} = (Ne^2/\epsilon_0 m)^{1/2}$. Around the (screened) bulk plasmon frequency $\omega_{\text{bp}} \equiv \omega_{\text{pl}}/\sqrt{\epsilon_\infty}$, the real part of the permittivity shows a transition from negative to positive values. Noble metals have carrier densities N exceeding 10^{22} cm^{-3} , therefore their bulk plasmon plasma frequency is located in the UV region. In contrast, highly doped semiconductors typically have electron densities below 10^{19} cm^{-3} and can be well described by the Drude model with a bulk plasmon plasma frequency in the THz range. Transparent conducting oxides (TCOs), with an electron density inbetween that of bulk metals and doped semiconductors, show a bulk plasmon frequency in the near-infrared. The resulting combination of a metal-like response in the infrared and a dielectric optical response in the visible region has stimulated application of TCOs as transparent electrical contacts and as heat reflecting windows. Recently, metal oxides such as indium-tin oxide (ITO) and aluminium-doped zinc oxide have received interest for their plasmonic response in relation to metamaterials and transformation optics.[8, 9] The plasma frequency can be tuned by controlling the electron density using electrical

or optical methods, opening up opportunities for near-infrared electro-optic or optical modulators [7, 10, 11] and sensing devices.[12, 13]

Pioneering studies by Franzen and co-workers have investigated the plasmonic response of ITO and ITO-gold hybrid structures in the metallic (negative epsilon) regime of ITO.[13] Next to a conventional surface plasmon polariton mode for thick ITO films, a new polariton mode associated with the bulk plasmon resonance was observed for 30 nm thin films. By using hybrid ITO-gold layers, the balance between the two types of plasmonic modes could be controlled. In analogy with metal nanoantennas, ITO and AZO colloidal nanoparticles and nanorods revealed pronounced surface plasmon resonances in the infrared range.[12, 14, 15]

Here, we explore the intermediate regime where ITO shows a dielectric response with a refractive index below that of vacuum. In this studies, we used commercial ITO slides (Lumtec) of 350-nm thickness with a sheet resistance of $5 \pm 1 \Omega/\text{square}$. Figure 1(a) shows the calculated dispersion relation for these ITO samples (blue line) using the Drude model with experimentally obtained parameters $m = 0.4m_e$, $\gamma_D = 0.2 \text{ PHz}$ [13] and $N = 1.13 \times 10^{21} \text{ cm}^{-3}$. The thin line (red) indicates the dispersion relation of light in vacuum. A low-index regime is observed in the frequency range between 0.24–0.27 PHz, which characterized by a superluminal phase velocity and a correspondingly reduced wavevector. The dielectric ENZ regime covers the range of (complex) wavevectors given by the condition $\text{Im} k_{\text{ITO}} < \text{Re} k_{\text{ITO}} < k_0$, as indicated by the shaded area in the dispersion relation. Figures of merit for the ENZ response are the refractive index $\text{Re} n_{\text{ITO}}$ and the propagation length in units of wavelength $\text{Re} n_{\text{ITO}}/2\text{Im} n_{\text{ITO}}$, as shown in Fig. 1(b). While the refractive index increases from 0.48 to 1.0 over the ENZ window, the propagation length of light in the ITO layer increases from 0.5 to 3.2 wavelengths.

Light incident on an interface between two media from the medium with the higher refractive index undergoes total internal reflection above a critical angle θ_{crit} . Similarly, at the interface between air and an ENZ medium,

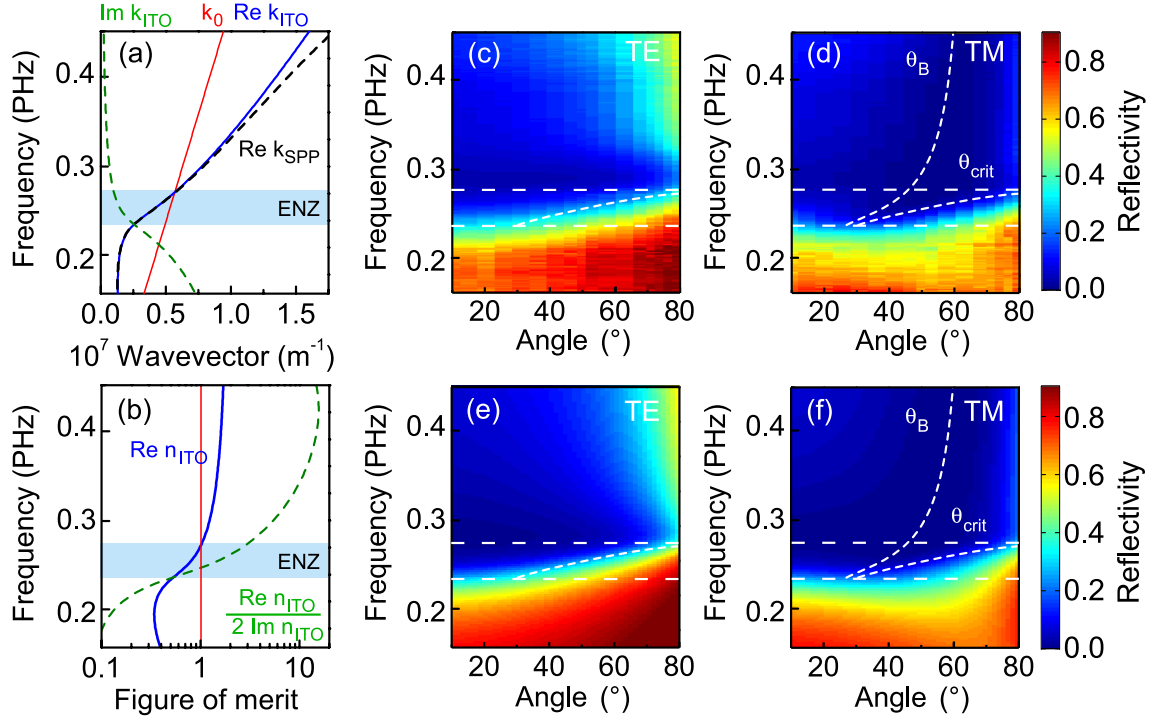


FIG. 1: (Color online) (a) Photon dispersion relations for air (red), ITO (blue) and the ITO-Au SPP (dash, black), with imaginary part for ITO (short dash, green). (b) Same for real refractive index $\text{Re} n_{\text{ITO}}$ and the propagation length in number of wavelengths, $\text{Re} n_{\text{ITO}}/2 \text{Im} n_{\text{ITO}}$. Reflectivity as a function of angle, with (white line) calculated TERF critical angle. Blue shaded area in (a) and dotted lines in (b) indicate epsilon-near zero (ENZ) regime.

a similar effect of total external reflection occurs. Total external reflection at grazing angles is a well-known phenomenon in x-ray optics, where it is commonly used in reflective focusing optics, waveguides, and surface analysis.[17] Figures 1(c,d) show the reflectivity of the ITO-glass slide for various angles of incidence for TM and TE polarizations. The dashed lines indicate the estimated positions of the critical and Brewster's angles θ_{crit} and θ_B in the absence of absorption, i.e. using $\theta_{\text{crit}} = \sin^{-1}(\text{Re} n_{\text{ITO}})$ and $\theta_B = \tan^{-1}(\text{Re} n_{\text{ITO}})$. The critical angle ranges between 30° and 90° . For both polarizations, an increase in reflectivity is observed in the ENZ regime above the critical angle. The exact definitions for θ_{crit} and θ_B lose validity in the presence of absorption, and for strong absorption they tend to shift toward larger angles.[18] To compare the exact behavior we calculated Fresnel's reflectivities using the Drude model with optimized free carrier density of $N = 1.13 \times 10^{21} \text{ cm}^{-3}$. The resulting Figs. 1(e,f) show good agreement with the experimental data and confirm the presence of total external reflection in the ENZ regime of ITO.

In order to assess the air-guiding effect associated with total external reflection in ITO, we changed the configuration to a planar waveguide by aligning two ITO-slides with a tunable separation of several hundred μm . The optical beam was focused to a spot of $50 \mu\text{m}$ in diameter using a focusing lens with numerical aperture of 0.02. By

tuning the space between the slides, we achieved up to 8 multiple reflections. The resulting transmission spectrum through the waveguide is shown in Fig. 1 for different angles of incidence. We identify three regimes, respectively at energies below, in, and above the ENZ regime. Below the ENZ window, the metallic reflectivity of ITO results in a weakly varying transmission of several percent. This transmission is low because of insertion losses as well as because of the limited single-pass reflectivity of up to 75% giving rise to a multi-pass transmission below 10%. Above the ENZ regime, the transmission contains contributions from the air-ITO and the ITO-glass interface, which are overall relatively small but increasing toward large angles of incidence. In the ENZ regime, large variations of the transmission are found when changing the angle of incidence by only a few degrees. A pronounced spectral dip is observed for TM polarization at angles below 80° , which is caused by a combination of reduced reflection of the ITO-air interface and increased absorption in the ITO layer. Above the critical angle, the waveguide transmission dramatically increases by more than three orders of magnitude around 0.25 PHz. These results indicate a potential application of TCO air-guided waves using total external reflection, for example in optical sensors or modulators.

Next, we investigated electromagnetic surface waves at the interface between ITO and gold in the ENZ regime. Surface plasmon polaritons (SPPs) on metal films are re-

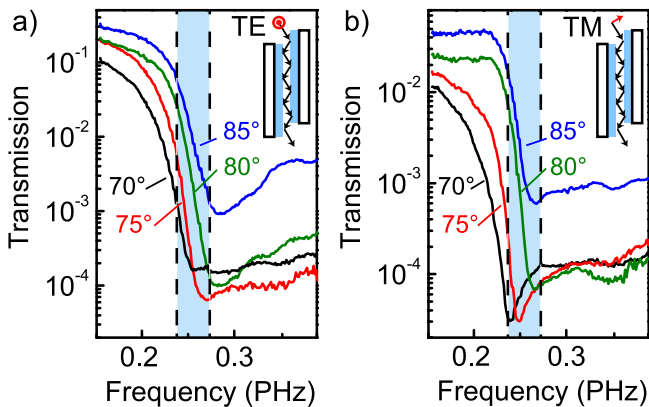


FIG. 2: (Color online) Transmission of air-guided ITO-cladded waveguide for 8 multiple reflections, for TE (a) and TM (b) polarizations and for angles of incidence between 70° and 85°. Blue shaded areas indicate epsilon-near zero (ENZ) regime.

ceiving enormous interest for their application in sensing and surface plasmon optics.[19] The SPP wavevector is given by

$$k_{\text{SPP}} = k_0 \left(\frac{\epsilon_d \epsilon_m}{\epsilon_d + \epsilon_m} \right)^{1/2}. \quad (2)$$

The permittivities of the metal ϵ_m and the dielectric ϵ_d both depend on frequency. The dashed black line in Fig. 1(a) shows the calculated SPP wavevector for the ITO-gold interface. The surface plasmon resonance is located at 0.618 PHz, outside the plotted window. For low energies, the SPP has a photon-like nature and its dispersion follows that of the ITO film.

For conventional SPPs occurring at the interface between a dielectric and metallic layer, the wavevector is larger than that of free-space radiation; therefore coupling to SPPs requires wavevector matching using a glass prism, grating, or near-field scattering object. The ENZ-regime, however, enables a new type of SPP mode at the interface of Au and ITO, which lies below the light line. Consequently, the SPP can directly couple to free-space radiation. Figure 3(a) shows the measured reflectivity of the 350-nm thick ITO layer coated with a 50-nm thick (continuous) Au film, for illumination through the ITO-side. A pronounced dip is observed around 0.25 PHz, which agrees well with the coupling angle obtained using $\theta_{\text{SPP}} = \sin^{-1}(k_{\text{SPP}}/k_0)$, which in this frequency range closely follows θ_{crit} . A cross section of the reflectivity spectrum at 65°, plotted in Fig 3(b) (solid line), shows a well-defined spectral dip with a quality factor of ~ 8.4 . The angular dispersion is very flat and covers a range of around 30° for which light can be coupled into the SPP mode at a frequency of 0.25 PHz.

The effect of an additional SiO₂ spacer layer between the ITO and Au layers is shown by the dashed line in Fig. 3(b). The refractive index of the spacer slightly increases the mode index of SPP, resulting in a redshift

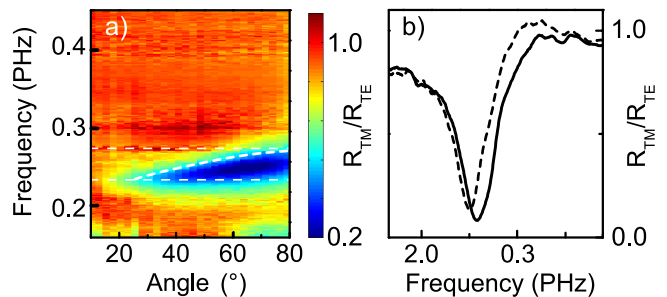


FIG. 3: (Color online) (a) Experimental reflectivity $R_{\text{TM}}/R_{\text{TE}}$ for the ITO-Au multilayer. (b) Spectra at 65° angle of incidence for a 350 nm ITO - 50 nm Au (solid) and 350nm ITO - 40 nm SiO₂ - 50 nm Au multilayer structures.

of the SPP dispersion. In addition a 10% narrowing is observed which we attribute to reduced losses in the dielectric layer. The possibility to include a spacer layer is of interest as it allows electrically isolating the gold film from the ITO and holds promise for incorporating active layers, or field-effect designs for electro-plasmonic modulation.[7, 10] Figure 3 shows that, even for a SiO₂ spacer layer of 40 nm thickness, the effective mode index of the SPP lies below unity and the SPP couples to free-space radiation.

As a demonstration of the functionality of the SPPs supported on the Au-ITO interface, we demonstrate ultrafast control over the plasmon mode using femtosecond pulsed laser excitation. Ultrafast control of plasmons is of interest for applications in optical switching.[20] Here we use the ultrafast response of the Au-ITO hybrid to produce a spectral shift of the plasmon mode. The nonlinear response was obtained using a regenerative amplifier with OPA (Coherent RegA), producing 220-fs laser pulses with a repetition rate of 250 kHz. Modulation of the probe pulses was detected using a lock-in amplifier to collect the modulation integrated over the ~ 0.01 PHz spectral bandwidth of the OPA output. Additionally a spectrometer could be used to resolve relative changes in the probe spectrum larger than 1%. Figure 4a-e show the nonlinear response of the ITO. The absolute probe signal with and without pump is shown in Fig. 4(a) for a pump-probe delay of 0.2 ps, with the equivalent differential reflectivity shown in Fig. 4(b) (solid line, black).[21] For TM-polarization, a bipolar differential reflectivity is observed, indicative of a redshift of the SPP resonance. The magnitude of the differential signal reaches up to 20% at a pump fluence of around 10 mJ/cm². In comparison, the TE polarization only shows a wavelength-independent negative contribution. The full spectral and time evolution of the pump-probe response is shown in Fig. 4d) and e). We note, apart from an ultrafast component, a thermal background with the same spectral shape due to buildup of heat in the sample over many repetition cycles. The nonlinearity is thus associated with significant energy injection, ruling out a Kerr-type nonlinearity. The nonlinear modulation of the SPP is therefore attributed

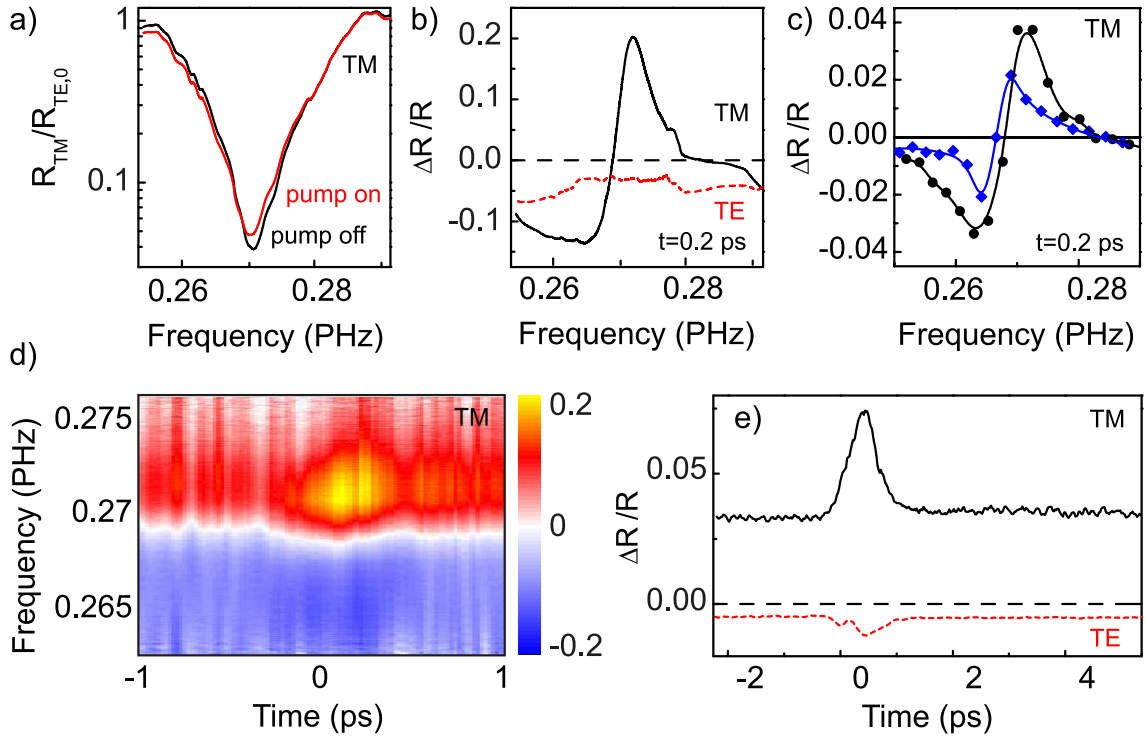


FIG. 4: (Color online) (a) Reflectivity R_{TM} with and without pump laser, normalized to intensity of TE without pump $R_{\text{TE},0}$. (b) Differential reflectivity $\Delta R/R$ for both TM (line, black) and TE (dash, red) polarizations and for pump-probe delay time of 0.1 ps, at pump fluence of 10 mJ/cm². (c) Comparison of $\Delta R/R$ for ITO-Au (dots, black) and ITO-SiO₂-Au (diamonds, blue) multilayers at pump fluence of 3 mJ/cm². (d) Spectral map of differential reflection for TM obtained using spectrometer, with (e) spectrally integrated pump-probe signal for TM (line, black) and TE (dash, red). (c) and (e) were measured using lock-in technique.

by ultrafast heating of the Au-ITO hybrid. Furthermore, the time-response of the TE-reflectivity indicates the presence of an additional small instantaneous contribution, possibly related to nondegenerate two-photon absorption, or to the instantaneous Kerr-nonlinearity of ITO.[22]

In hybrid nanostructures, hot-electron transfer may form a new mechanism for enhancing the nonlinear response.[11, 23] To investigate this contribution, we tested the response of a multilayer consisting of 50 nm Au, 20 nm SiO₂ and 350 nm ITO. It was found that the damage threshold of the Au layer in this sample was substantially lower than the Au-ITO sample by a factor of three. The reduced pump power required the use of more sensitive lock-in detection, resulting in the frequency dependent response shown in Fig. 4(c). We find qualitatively the same response for the two Au-ITO (dots) and Au-SiO₂-ITO (diamonds, blue) samples, indicating that in both cases, the signal is governed by a redshift of the SPR. For the Au-SiO₂-ITO multilayer, the signal is reduced by a factor two. The combination of an increased damage threshold and higher nonlinear response in the Au-ITO hybrid is consistent with the ultrafast hot-electron transfer mechanism which lowers the stress of the Au-film and increases the hybrid nonlinear

response.

In conclusion, we have demonstrated new properties of ITO in the regime characterized by a refractive index below unity (Epsilon Near-Zero). The ITO layer shows pronounced total external reflection which can be used to obtain waveguiding of light using air as the high-index medium. As the refractive index and thus the external reflection condition strongly depends on carrier density, this effect may be useful for applications in optical sensing. In addition, we have identified a new surface plasmon polariton mode at the interface between ITO and gold. The plasmon polariton is observed to couple strongly to free-space radiation without requiring additional phase matching, which is attributed to the strongly reduced wavevector in the ENZ regime. We have demonstrated that this mode can be controlled on ultrafast time scale, opening up potential application in optical switching. Future work may identify other applications of this new plasmon mode may be useful for applications such as outcoupling of light from emitters, local field enhancement, or strong light absorption in energy harvesting applications.

This work was supported by the EPSRC through grants EP/J011797/1 and EP/J016918/1.

-
- [1] S. Enoch, G. Tayeb, P. Sabouroux, N. Guérin and P. Vincent, *Phys. Rev. Lett.* **89**, 213902 (2002).
- [2] Andrea Alù, M. G. Silveirinha, A. Salandrino, and N. Engheta, *Phys. Rev. B* **75**, 155410 (2007).
- [3] R. J. Pollard, A. Murphy, W. R. Hendren, P. R. Evans, R. Atkinson, G. A. Wurtz, and A. V. Zayats, *Phys. Rev. Lett.* **102**, 127405 (2009).
- [4] B. T. Schwartz, R. Piestun, Waveguiding in air by total external reflection from ultralow index metamaterials, *Appl. Phys. Lett.* **85**, 1 (2004).
- [5] M. Silveirinha, N. Engheta, *Phys. Rev. Lett.* **97**, 157403 (2006).
- [6] E.J.R. Vesseur, T. Coenen, H. Caglayan, N. Engheta, and A. Polman, *Phys. Rev. Lett.* **109**, in press (2012)
- [7] Z. Lu, W. Zhao, and K. Shi, *IEEE Phot. J.* **4**(3), 735 (2012).
- [8] P. West, S. Ishii, G. Naik, N. Emani, V. M. Shalaev, A. Boltasseva, *Laser Photon. Rev.* **4**, 795 (2010).
- [9] M. A. Noginov, L. Gu, J. Livenere, G. Zhu, A. K. Pradhan, R. Mundle, M. Bahoura, Yu. A. Barnakov, V. A. Podolskiy, *Appl. Phys. Lett.* **99**, 021101 (2011).
- [10] E. Feigenbaum, K. Diest and H. A. Atwater, *Nano Lett.* **10**, 2111 (2010).
- [11] M. Abb, P. Albella, J. Aizpurua, O. L. Muskens, *Nano Lett.* **11**, 2457:2463 (2011).
- [12] S. Q. Li, P. Guo, L. Zhang, W. Zhou, T. W. Odom, T. Seideman, J. B. Ketterson, R. P. H. Chang, *ACS Nano* **5**, 9161 (2011).
- [13] S. H. Brewer and S. Franzen, *J. Phys. Chem B* **106**, 12986 (2002); S. Franzen, *J. Phys. Chem. C* **112**, 6027 (2008); S. Franzen, C. Rhodes, M. Cerruti, R. W. Gerber, M. Losego, J.-P. Maria and D. E. Aspnes, *Opt. Lett.* **34**, 2867 (2009).
- [14] M. Kanehara, H. Koike, T. Yoshinaga, T. Teranishi, *J. Am. Chem. Soc.*, **131**, 1773617737 (2009).
- [15] R. Buonsanti, A. Llordes, S. Aloni, B. A. Helms, D. J. Milliron, *Nano Lett.*, **11**, 47064710 (2011).
- [16] Y. Xu and H. Chen, *Appl. Phys. Lett.* **98**, 113501 (2011).
- [17] B. Aschenbach, *Rep. Prog. Phys.* **48**, 579 (1985).
- [18] G. H. Meeten, *Meas. Sci. Technol.* **8**, 728 (1997).
- [19] W. L. Barnes, A. Dereux, T. W. Ebbesen, *Nature* **424**, 824-830 (2003).
- [20] K. F. MacDonald, Z. L. Sámson, M. I. Stockman, and N. I. Zheludev, *Nature Photonics* **3**, 55, (2008).
- [21] We note that the resonance position is shifted by 0.1 PHz with respect to Fig. 3 because a different sample was used with slightly different carrier density.
- [22] H. I. Elim, W. Ji, F. Zhu, *Appl. Phys. B* **2006**, **82**, 439-442
- [23] M. Kauranen and A. V. Zayats, *Nat. Photon.* **6**, 737-748 (2012).